Remote Sensing of Environment 196 (2017) 101–112

Contents lists available at ScienceDirect

Remote Sensing of Environment

journal homepage: www.elsevier.com/locate/rse

Validation and scaling of soil moisture in a semi-arid environment: SMAP validation experiment 2015 (SMAPVEX15)

Andreas Colliander [a,*], Michael H. Cosh [b], Sidharth Misra [a], Thomas J. Jackson [b], Wade T. Crow [b], Steven Chan [a], Rajat Bindlish [c], Chunsik Chae [a], Chandra Holifield Collins [d], Simon H. Yueh [a]

[a] Jet Propulsion Laboratory, California Institute of Technology, Pasadena, CA, USA
[b] USDA Agricultural Research Service, Hydrology and Remote Sensing Lab, Beltsville, MD, USA
[c] NASA Goddard Space Flight Center, Greenbelt, MD, USA
[d] USDA Agricultural Research Service, Southwest Watershed Research Center, Tucson, AZ, USA

ARTICLE INFO

Article history:
Received 9 November 2016
Received in revised form 8 April 2017
Accepted 23 April 2017
Available online 8 May 2017

Keywords:
SMAPVEX15
PALS
SMAP
Soil moisture

ABSTRACT

The NASA SMAP (Soil Moisture Active Passive) mission conducted the SMAP Validation Experiment 2015 (SMAPVEX15) in order to support the calibration and validation activities of SMAP soil moisture data products. The main goals of the experiment were to address issues regarding the spatial disaggregation methodologies for improvement of soil moisture products and validation of the *in situ* measurement upscaling techniques. To support these objectives high-resolution soil moisture maps were acquired with the airborne PALS (Passive Active L-band Sensor) instrument over an area in southeast Arizona that includes the Walnut Gulch Experimental Watershed (WGEW), and intensive ground sampling was carried out to augment the permanent *in situ* instrumentation. The objective of the paper was to establish the correspondence and relationship between the highly heterogeneous spatial distribution of soil moisture on the ground and the coarse resolution radiometer-based soil moisture retrievals of SMAP. The high-resolution mapping conducted with PALS provided the required connection between the *in situ* measurements and SMAP retrievals. The *in situ* measurements were used to validate the PALS soil moisture acquired at 1-km resolution. Based on the information from a dense network of rain gauges in the study area, the *in situ* soil moisture measurements did not capture all the precipitation events accurately. That is, the PALS and SMAP soil moisture estimates responded to precipitation events detected by rain gauges, which were in some cases not detected by the *in situ* soil moisture sensors. It was also concluded that the spatial distribution of the soil moisture resulted from the relatively small spatial extents of the typical convective storms in this region was not completely captured with the *in situ* stations. After removing those cases (approximately 10% of the observations) the following metrics were obtained: RMSD (root mean square difference) of 0.016 m^3/m^3 and correlation of 0.83. The PALS soil moisture was also compared to SMAP and *in situ* soil moisture at the 36-km scale, which is the SMAP grid size for the standard product. PALS and SMAP soil moistures were found to be very similar owing to the close match of the brightness temperature measurements and the use of a common soil moisture retrieval algorithm. Spatial heterogeneity, which was identified using the high-resolution PALS soil moisture and the intensive ground sampling, also contributed to differences between the soil moisture estimates. In general, discrepancies found between the L-band soil moisture estimates and the 5-cm depth *in situ* measurements require methodologies to mitigate the impact on their interpretations in soil moisture validation and algorithm development. Specifically, the metrics computed for the SMAP radiometer-based soil moisture product over WGEW will include errors resulting from rainfall, particularly during the monsoon season when the spatial distribution of soil moisture is especially heterogeneous.

© 2017 Elsevier Inc. All rights reserved.

1. Introduction

The SMAP post-launch Calibration/Validation (Cal/Val) plan is intended to assess the quality of the mission products and to support analyses that lead to their improvement. A suite of complementary methodologies employed together will result in a robust global assessment (Jackson et al., 2013). These methodologies include the utilization of core validation sites (Colliander et al., 2017), sparse networks (Chen et al., 2017), other satellite data products (Burgin et al., 2017), model-based data products (Pan et al., 2016), and field campaigns. Field campaigns, in particular those using aircraft-based higher-resolution satellite sensor simulators, play an important role in satellite product Cal/Val by providing detailed ground truth; however, they are limited in

* Corresponding author.
E-mail address: andreas.colliander@jpl.nasa.gov (A. Colliander).

http://dx.doi.org/10.1016/j.rse.2017.04.022
0034-4257/© 2017 Elsevier Inc. All rights reserved.

their spatial extent and duration by logistics and costs. Specific SMAP science activities that can be addressed using an aircraft-based campaign include: validating spatial disaggregation of satellite soil moisture or brightness temperatures, investigating and resolving anomalous observations and products (such as large deviations from *in situ* estimated soil moistures), defining site specific upscaling, understanding the effects and contribution of heterogeneity on coarser resolution retrievals, and providing correlative analysis of L1 data product calibration.

SMAPVEX15 was the first SMAP post-launch field campaign and was designed to address the issues noted above. Post-launch field experiments were also carried out in Australia (Ye et al., 2016) in 2015. The SMAP post-launch field campaigns follow a series of pre-launch field campaigns carried out in USA, Canada and Australia (Colliander et al., 2012; Panciera et al., 2014; Magagi et al., 2013; McNairn et al., 2015). The timing and location of the SMAPVEX15 campaign was based on the needs to capture a range of soil moisture conditions in a short period of time and to observe well-defined and highly heterogeneous soil moisture spatial patterns that would provide a clear validation of disaggregation approaches. This led to the selection of a core validation site in southeast Arizona during the summer monsoon season. The campaign was conducted between August 1 and 18, 2015. This was shortly after the loss of the SMAP radar; therefore, the campaign objectives shifted from the validation of the SMAP disaggregation techniques and the other goals were reprioritized. However, the data set will be of value for the validation of future disaggregation approaches.

This paper focuses on the investigation of the sub-pixel soil moisture heterogeneity as measured with the PALS (Passive Active L-band System) airborne radiometer as it scales to the SMAP data products. The objective of the paper is to establish the correspondence and relationship between the highly heterogeneous spatial distribution of soil moisture on the ground and the coarse resolution radiometer-based soil moisture retrievals of SMAP. The high-resolution mapping conducted with PALS provided the required connection between the *in situ* measurements and SMAP retrievals. SMAPVEX15 was the first major campaign to utilize the conical scanning mode of the PALS instrument installed on a DC-3 aircraft (Misra et al., 2017). Data collected with PALS radar are available as well, but because of the failure of the SMAP radar this study is solely focused on the radiometer data. The data collected by PALS on multiple days were used to produce high-resolution brightness temperature data sets. The PALS radiometer observations were then translated into high-resolution soil moisture retrievals that were validated using ground-based observations. The PALS brightness temperature and validated soil moisture were aggregated to the spatial resolution of the SMAP L2 radiometer-based soil moisture product (36 km). These soil moisture estimates were compared to each other and to up-scaled *in situ* soil moistures. The comparison of the *in situ* soil moistures at 5-cm depth and the radiometer-based soil moisture, which is sensitive to moisture starting from the top surface, also gives a perspective on the vertical distribution of soil moisture in addition to the horizontal distribution captured by the PALS measurements. The study focuses on the area of the WGEW validation pixel, which is used for SMAP data product validation (Keefer et al., 2008; Colliander et al., 2017).

2. Site description

The SMAPVEX15 campaign took place in southeastern Arizona, encompassing several experimental sites and ranges operated by the United States Department of Agriculture (USDA) Agricultural Research Service (ARS) Southwest Watershed Research Center in Tucson, AZ, and the University of Arizona. Fig. 1 shows the domain along with the specific watersheds and experimental ranges included in the study. The Walnut Gulch Experimental Watershed (Moran et al., 2008), located in the eastern portion of the domain has been the location of numerous soil moisture field experiments in the past, including MONSOON '90 (Kustas et al., 1994) and SMEX04 (Soil Moisture Experiment in 2004) (Bindlish et al., 2008). It is a semi-arid region with an annual average precipitation of 312 mm, approximately 60% of it coming during the summer monsoon season, July to September (Goodrich et al., 2008). The majority of this monsoon rainfall occurs within highly localized convective storms – leading to large amounts of spatial variability in rainfall accumulations. During August of 2015, the average air temperature was 25 °C and the average relative humidity was 53%. The Santa Rita Experimental Range (SRER) in the western portion of the study domain is a more traditional desert landscape dominated by cactus and large shrubs. In the center of the SMAPVEX15 domain is a grassland

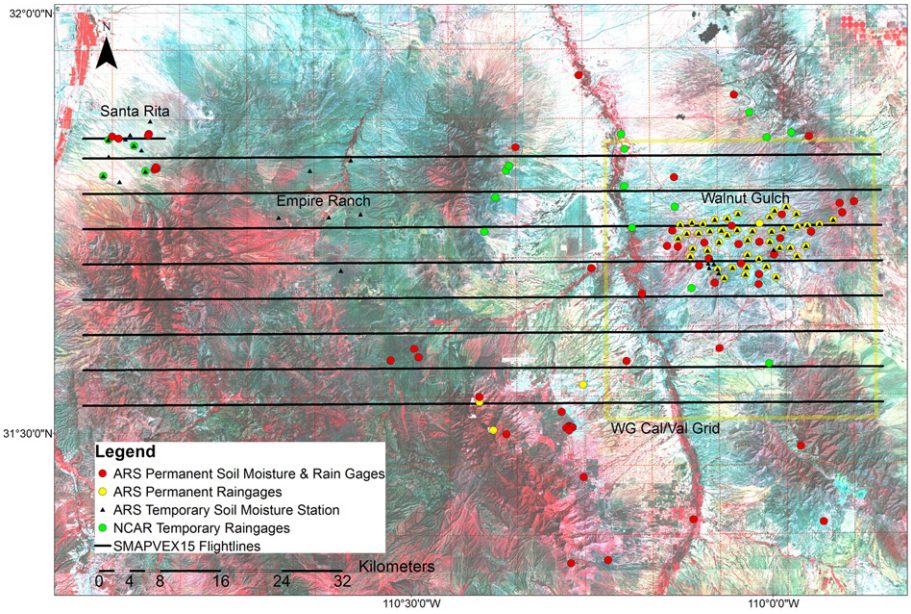

Fig. 1. SMAPVEX15 campaign domain and the PALS flight lines (black). The underlying image is a false color image of Landsat 8 from 8/3/15 (West) and 8/12/15 (East).

area called Empire Ranch. This is an active cattle ranch (administrated by the U.S. Bureau of Land Management) with rolling topography.

3. *In situ* data collection and processing

There were three primary methods of soil moisture data collection during the SMAPVEX15 field campaign: the permanent *in situ* network, a temporary *in situ* network, and concurrent manual physical sampling. The WGEW has a long-term permanent soil moisture and soil temperature network that is collocated with a more densely instrumented precipitation gauge network. There are 19 soil moisture stations within the WGEW. Throughout the entire SMAPVEX15 study domain, USDA ARS operates a total of 52 soil moisture stations. These stations record precipitation and soil moisture and soil temperature every 20 min at a depth of 5 cm with a Stevens Water Hydra Probe (mention of this commercial product does not constitute an endorsement), installed horizontally. This provides an integrated estimate for soil moisture from approximately 3 to 7 cm and is commonly used as an estimate of the surface layer soil moisture. Precipitation gauges are a weighing type designed especially for the high intensity rainfall that is received during the monsoon season. From July to October of 2015, a temporary *in situ* network of 66 soil moisture and soil temperature stations was deployed in the region. This network consisted of a single soil moisture probe installed at 5-cm depth horizontally, which is identical to the permanent network configuration. The final element of the ground-based soil moisture data collection was concurrent physical sampling, conducted by field sampling teams during the intensive observation period (IOP) from August 1 to 18. Seven teams of two samplers, visited a total of 80 network sites on every aircraft flight day and collected dielectric-based probe measurements of soil moisture. To do this, the probe was inserted vertically into the top of the soil at three locations, randomly selected near each network site. In addition, a gravimetric sample of the soil was collected and combined with site specific bulk density estimates to produce site specific calibration equations. The samples were collected at locations around the permanent and temporary stations, within several meters, but not within 1 m, so as not to interfere with the installation. When combined with a bulk density estimate for each domain (and data available from the SMEX04 dataset), this produced a concurrent soil moisture estimate for the seven days of flights. An overall RMSE of 0.02 m^3/m^3 volumetric soil moisture was achieved following the protocols established in Cosh et al. (2005) and Rowlandson et al. (2013). This data serves as the ground truth for both the temporary network operations and scaling efforts.

Rain radar coverage from the Tucson NEXRAD station is available within the center part of the of SMAPVEX15 domain. However, topographic beam blockage is significant along the western and eastern edges of the domain (particularly to the east of the Whetstone mountain range in the vicinity of Tombstone). Such blockage severely limits the ability of the Tucson NEXRAD to characterize rainfall accumulations. These gaps are partially compensated for by a large permanent rain gauge network within both the SRER and WGEW sites (due to extensive ground monitoring activities conducted by BLM and USDA ARS, respectively). However, significant gaps still exist in the outlying areas surrounding both sites. In order to (partially) fill these gaps, 18 tipping bucket rain gauges (Texas Electronics Model TE525-USW) were deployed during the last two weeks of July 2015 around the SRER and WGEW sites. During August 2015, these gauges were serviced periodically for data retrieval, cleaning of screens and tipping buckets, spot calibration and re-leveling. All gauges were removed in early September 2015.

The cumulative error of the network is calculated by accounting for the uncertainty in both the sensor calibration and the error in representing the spatial distribution of soil moisture. For the former, the upper limit of the sensor calibration for the permanent and temporary stations is used ($\sigma_{sensor} = 0.03$ m^3/m^3 based on manufacturer; not to be confused with the manual probe calibration mentioned above) and for the latter the analysis presented in Famiglietti et al. (2008) is applied. The error is computed as the squared sum of these two components:

$$\epsilon = \sqrt{\left(\frac{\sigma_{sensor}}{\sqrt{N}}\right)^2 + \left(\frac{\sigma_{spatial}\, t_{0.975,N}}{\sqrt{N}}\right)^2} \quad (1)$$

where N is the number of stations within a pixel, $\sigma_{spatial}$ is the standard deviation of the soil moisture within each pixel on each day derived from the PALS measurements, and $t_{0.975,N}$ is the inverse of Student's t-distribution for 0.975 probability (95% confidence interval) with N degrees of freedom. It should be noted that for the original configuration of the soil moisture observation network the error was found to be 0.01 m^3/m^3 (Cosh et al., 2008).

4. Airborne measurements

4.1. PALS brightness temperature calibration

The PALS instrument collects coincident (in time and place) radar and radiometer measurements (Wilson et al., 2001; Misra et al., 2017). Both measurements are obtained through the same antenna in a fast-switching sequence. PALS has been used in several soil moisture studies in the past (*e.g.*, Njoku et al., 2002; Narayan et al., 2004; Bindlish et al., 2009; Colliander et al., 2012, 2015, 2016a; Barber et al., 2016). During SMAPVEX15, PALS was installed on a DC-3 aircraft. In its 2015 configuration PALS employed a lightweight antenna with a 21° beamwidth (Yueh et al., 2008), which had been upgraded to include a scanning mechanism. The PALS antenna was attached to a scan head under the fuselage of the aircraft allowing a full 360° conical scan at 40° incidence angle, which matches the observing angle of SMAP. This design results in a footprint of 1100 m (along scan) by 1500 m (radially) on the ground with an effective resolution of about 1200 m (square root of the area of the footprint ellipse) for the flights at 2300 m altitude above ground.

The operation of the PALS radiometer is based on a two-reference switching scheme (Wilson et al., 2001); this design was adopted for the radiometers deployed by the SMAP (Piepmeier et al., 2017) and Aquarius missions (Le Vine et al., 2007). One of the references is a matched load and the other one is a noise diode. These two loads allow the removal of internal gain and offset fluctuation of the radiometer chain during operation. The brightness temperature at the input of the antenna is computed using the principles presented by Tanner et al. (2003). In general, water bodies are reliable and widely used calibration targets for airborne low-frequency radiometers. However, for SMAPVEX15 suitable water bodies were not available in the vicinity of the flight path (long transit times limited the flight range available for water body calibrations) for tracking co-incident relative calibration with science flights. In order to test the repeatability of the calibration an external absorber load at ambient temperature and a sky reflection were measured before and after each flight. These external calibration measurements were suitable for tracking major relative calibration changes in the radiometer. A separate lake overflight was conducted to tie the relative target measurements to absolute values. Fig. 2 shows the vertically polarized brightness temperature for each PALS flight during SMAPVEX15.

4.2. PALS derived soil moisture

The soil moisture is retrieved following the standard τ-ω-h formulation, *e.g.*, (Njoku and Entekhabi, 1996) where the top of the

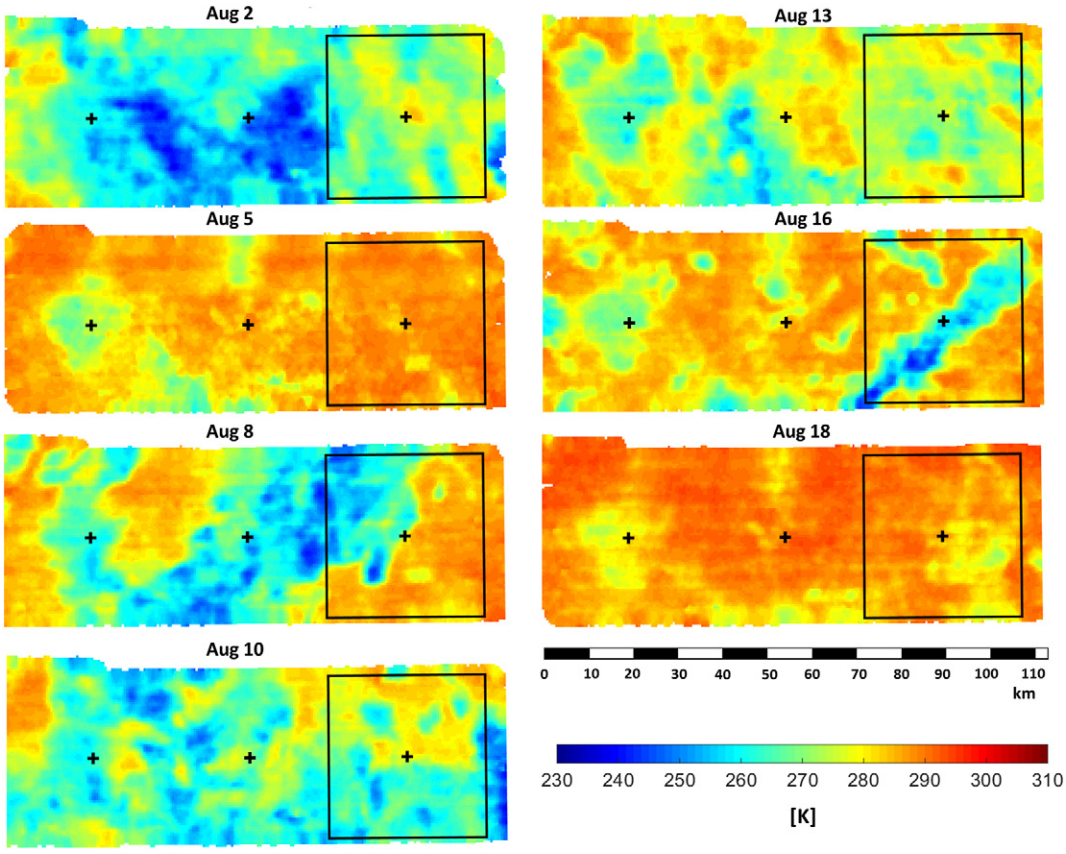

Fig. 2. Vertically polarized PALS brightness temperature for each flight in SMAPVEX15. The black box denotes the WGEW validation pixel, and the crosses mark the center of each SMAP 36-km pixel (labeled P1 through P3 going from west to east) within the domain.

vegetation brightness temperature is modeled using roughness corrected reflectivity (r_{soil}), vegetation opacity (τ) and vegetation scattering parameter (ω):

$$T_{B,p}^{TOV} = (1-r_{soil,p})T_{soil}e^{-\tau_p} + T_{veg}(1-\omega_p)(1-e^{-\tau_p}) + T_{veg}(1-\omega_p) \times (1-e^{-\tau_p})r_{soil,p}e^{-\tau_p} \quad (2)$$

where the first term corresponds to the ground emission through the vegetation, the second term to the vegetation emission, and the third term to the vegetation emission dwelling downward and then reflected from the ground and propagated through the vegetation. For roughness correction, the classical model adopted from Choudhury et al. (1979) is used:

$$r_{soil,p} = r_{0,p}e^{-h_{0,p}cos^2(\theta)}, h_{0,p} = (2\sigma k)^2, \quad (3)$$

where $r_{0,p}$ is the flat surface reflectivity; θ is the incidence angle; σ is the root mean square deviation of the surface height, and k is the wave number in free space (29.62 1/m at 1.4135 GHz). The smooth surface reflectivity is related to soil dielectric constant through the Fresnel reflection coefficient. The soil dielectric constant is related to soil moisture using the Mironov model (Mironov et al., 2009), which has been found to perform somewhat better than alternatives in radiometer-based soil moisture retrieval applications (Bircher et al., 2012; Srivastava et al., 2015).

In order to precisely translate measured brightness temperature to emissivity the physical temperature distribution in this layer is required (Njoku and Kong, 1977). However, because a precise, concurrent and complete vertical and spatial distribution of temperatures is very difficult to measure, we used the temperature measurements that were collected in the experiment to develop estimates for the soil temperature, represented by T_{soil} in Eq. (2). Specifically, we applied the 5-cm depth soil temperature measurements from the permanent soil moisture observation network to estimate the soil temperature. The soil temperature measurements were averaged and this value, at the time of the PALS flights, was used as T_{soil}. It is acknowledged that the deviation from the actual temperature profile introduces an error into the modeled brightness temperature. We also used the model forecast surface temperature provided as part of the SMAP product in the PALS soil moisture retrieval to facilitate additional comparisons between SMAP and PALS soil moistures at the 36-km scale. This value is computed using a combination of GMAO GEOS-5 layer 1 and layer 2 soil temperatures (O'Neill et al., 2016).

The vegetation opacity was derived by using a linear relationship defined by the vegetation water content (VWC) and an empirical parameter b_p (Kirdiashev et al., 1979; Jackson and Schmugge, 1991):

$$\tau_p = \frac{b_p W}{cos(\theta)} \quad (4)$$

where W is the vegetation water content. For consistency in the comparisons with respect to the SMAP soil moisture retrievals we applied the same VWC as SMAP does in its radiometer-based algorithm (Chan et al., 2013). The parameter b_p was given a value of 0.1 based on previous studies (Chan et al., 2016). The physical temperature of the vegetation was estimated from the thermal infrared measurements conducted along with the PALS measurements. The vegetation scattering parameter was assumed to be small ($\omega_p = 0.05$) as per Chan et al. (2016).

The soil moisture was retrieved on a 500-m grid, which is based on the 1-km SMAP grid. The SMAP products use Equal-Area Scalable Earth grid ver. 2 (EASE-2) (Brodzik et al., 2012). The 500-m grid will satisfy the Nyquist sampling criterion (*e.g.*, Chapter 3 in Smith, 1997) in the spatial domain for the 1200-m footprint PALS brightness temperature measurements. The resolution of the soil moisture is driven by that of

the PALS brightness temperature and is, therefore, also about 1200 m. We also used the same ancillary data as the SMAP L2SMP for land cover and soil texture (clay and sand fraction), as well as NDVI (normalized difference vegetation index) for vegetation water content (VWC) determination. The data were re-gridded onto the 500-m grid for processing. The PALS soil moisture retrieval algorithm minimizes the difference between modeled and measured brightness temperature in order to estimate the soil moisture for each pixel.

Fig. 3 shows the PALS-derived soil moisture for the entire domain on each flight day. The retrieved soil moisture maps are heavily influenced by the precipitation patterns resulting from the North American Monsoon (Adams and Comrie, 1997). The soil moisture pattern was highly variable from day to day, which was one of the goals of the experiment: to collect data with highly heterogeneous soil moisture conditions within SMAP footprints for testing disaggregation algorithms (see Section 1).

The uncertainty of the PALS soil moisture retrievals was estimated using the forward model described above. The parameter uncertainties applied in Monte Carlo simulations are listed in Table 1. The simulation was carried out for each retrieved soil moisture value.

Table 1
Uncertainty of the parameters used in the simulation to estimate the soil moisture retrieval error.

Parameter	Uncertainty
T_{Bp}	1 K
T_{soil}	3 °C
T_{veg}	5 °C
VWC	10%
h_p, b_p, ω_p	10%
Sand and clay fraction	10%

5. SMAP observations

In this investigation we examined both the SMAP radiometer brightness temperature measurements (Level 1) (Piepmeier et al., 2016) and the radiometer-based soil moisture retrievals, Level 2 Soil Moisture Passive (L2SMP) product (O'Neill et al., 2016). Details of the SMAP L2SMP algorithm are presented in Chan et al. (2016). The baseline algorithm uses vertically polarized brightness temperature and a single channel algorithm (Jackson, 1993) based on the τ-ω-h model presented in (1). This means the PALS algorithms described in Section 4.2 is very similar to the L2SMP baseline algorithm. The input brightness temperature is corrected for atmospheric effects, the antenna pattern and water bodies (which are not present in the experiment domain). The soil moisture retrieval takes place on the SMAP 36-km EASE-2 grid. Because the grid samples the ground in large intervals of 36-km, SMAP developed an additional process for retrieving the 36-km soil moisture also in offset intervals of 3-km. This so-called "validation grid" processing allows placing the 36-km retrieval pixels optimally with respect to *in situ* stations to reduce uncertainties arising from misalignment of the retrieval and the ground-based reference. A centered validation grid pixel was defined over the WGEW and these SMAP data will be compared to the PALS observations and *in situ* measurements. The analysis here focuses on the morning overpasses, which is the nominal observation time for SMAP (equatorial overpass at 6 AM local solar time). The expectation is that early in the morning the surface and vegetative thermal conditions are more consistent with isothermal assumptions made in the retrieval algorithm (O'Neill et al., 2016).

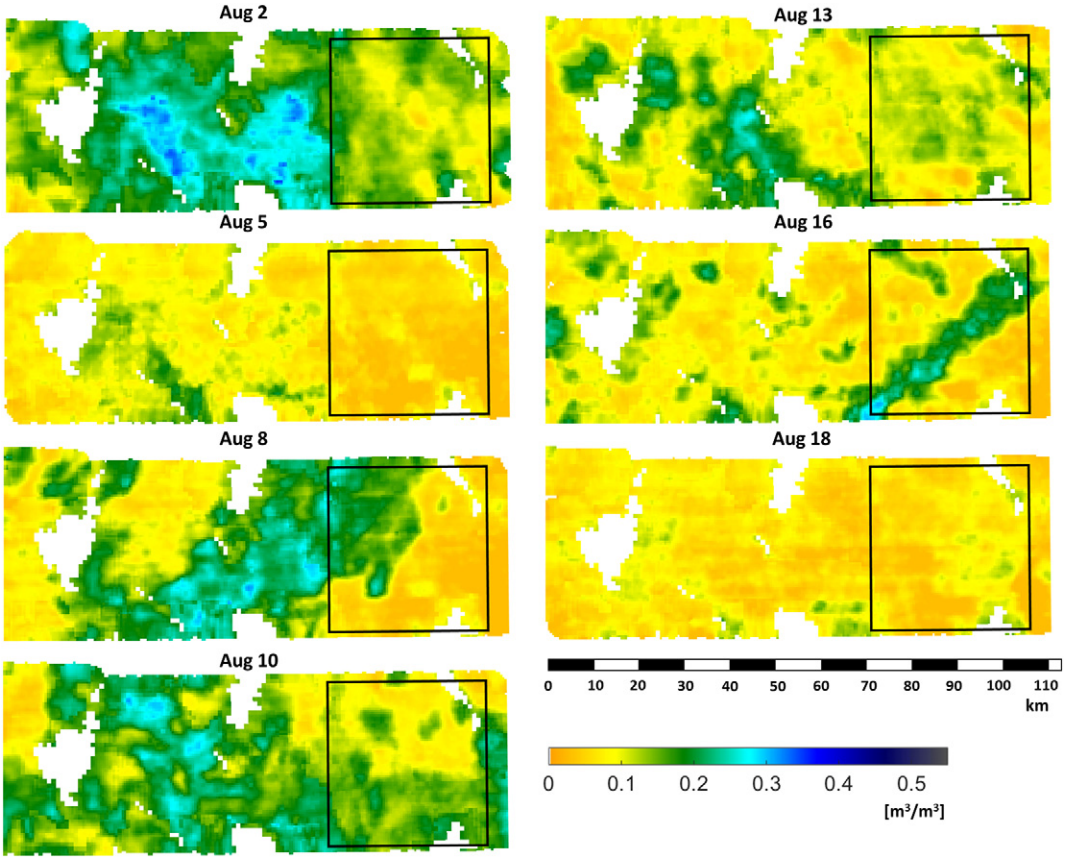

Fig. 3. Soil moisture maps derived from PALS brightness temperature for each flight in SMAPVEX15. The black box denotes the WGEW validation pixel. The blanked areas are due to the mountains.

6. Results

6.1. Brightness temperature observations

In addition to actual discrepancies in the calibration of the radiometers, there are several other factors that can cause both systematic and time-dependent differences in the comparison of airborne and spaceborne brightness temperature measurements. An obvious one is the timing of the observations: the dielectric constant of soil (soil moisture) and surface temperature can vary strongly over time, especially in a near desert environment like Walnut Gulch. Another important factor is differences in the area contributing to the observations. The SMAP antenna, like any real aperture radiometer antenna, has a main beam that is larger than the typically applied 3-dB footprint (in the SMAP L1 radiometer processing the effect of side lobes is compensated for, see Piepmeier et al., 2016). Hence, if the airborne measurements do not cover the entire area captured by the main beam, it is expected that there will be some additional uncertainty in the comparison. This uncertainty is a function of the brightness temperature heterogeneity within the actual footprint. Furthermore, the shape of antenna pattern affects how different parts of the area within the footprint are weighted. Therefore, brightness temperature heterogeneity – both inside and outside – of the 3-dB footprint may cause the spaceborne and airborne brightness temperature to differ.

In order to compare PALS and SMAP brightness temperatures, the SMAP brightness temperature over the experiment domain was obtained from the validation grid processing (see Section 5) for three pixels, whose centers are displayed in Fig. 2. The PALS measurements were averaged for each pixel using Gaussian weighting so that the weight decreases with distance from the pixel center and reduces to about half at a distance of 20 km. This approximates the effective antenna pattern, which is the result of the brightness temperature averaging in the L1C_TB processing (Chan et al., 2014). In addition, the arithmetic average of the PALS brightness temperature was computed within the boundaries of the 36-km pixels. There was <1.5 h difference between the PALS mean acquisition times over the pixel areas and the SMAP overpass time on each day; in most cases the PALS mean acquisition time was earlier than the SMAP overpass time. This translates to soil temperature differences that are in most cases <1 °C based on soil temperature averages obtained from the permanent *in situ* stations. Fig. 4 shows the PALS brightness temperature averages compared to the SMAP brightness temperatures over each pixel. The PALS brightness temperature computed with weighted average corresponded to SMAP somewhat better than the arithmetic average over the pixel areas. In particular the difference was notable in the cases when there is heterogeneity around the pixel edges. This was expected because the weighted average extends over the pixel boundaries. Overall, the comparison showed very similar trends in the PALS and SMAP brightness temperature records. Fig. 5 shows the scatterplot of the PALS brightness temperature obtained through Gaussian weighting and the SMAP brightness temperature. The error bars in the figure show the standard of brightness temperature in the pixel as determined from the PALS 1-km measurements. The overall mean difference between SMAP and Gaussian-weighted PALS brightness temperatures was very small for each pixel at the vertical polarization (ranging from −0.3 K to 1.3 K from pixel to pixel). For the horizontal polarization a larger overall mean difference was observed (ranging from −6.0 K to −11.0 K). These comparisons will be revisited once all calibration information from the lake flights and ground measurements are accounted for (see Section 4.1). For the purposes of this paper, the vertically polarized brightness temperature was used directly without compensating for the difference. The strong correlation between PALS and SMAP brightness temperatures supports the utilization of PALS brightness temperature for retrieving high-resolution soil moisture within the SMAPVEX15 domain to investigate effects of spatial soil moisture dynamics at sub-footprint scales of SMAP.

6.2. PALS vs. in situ soil moisture

In this section the PALS derived soil moisture is compared to *in situ* soil moisture measurements. In order to avoid comparing point measurements to PALS soil moisture values estimated over larger grids, a set of five 3-km validation pixels containing four or more *in situ* sensors was defined. Fig. 6(f) shows the layout of the stations (both permanent and temporary stations, see Section 3) and the five pixel boundaries with the day three and day six PALS soil moisture as the background. The 3-km grid is based on the SMAP EASE-2 grid. Fig. 6(a) through Fig. 6(e) show the PALS retrievals with the *in situ* measurement time-series. The plots show the averaged *in situ* soil moisture, the soil moisture of each individual station, an average of manual samples collected at each station, and the average precipitation. Fig. 7 shows the scatterplot of PALS soil moisture retrievals *versus* the *in situ* estimates for the pixels, and Table 2 shows the metrics for the PALS retrievals with respect to the *in situ* station soil moisture. Overall, the PALS retrievals corresponded well to the *in situ* average, and the manually sampled soil moisture corresponded well to the permanent and temporary station values; in particular, the trends of the soil moisture evolution were captured. The most notable exceptions occurred on day three in pixels 1 and 4 at stations P04 and P09, respectively. In the first case, the manual sample remained dry while the station responded to the rain event. In the second case, the manual sample responded to a rain event while the station remained dry. For pixels 1 through 4 there was one outlier for each pixel where PALS overestimated the soil moisture with respect to the station measurements. In each case, however, there was at least one station, which showed an increase in soil moisture and/or a precipitation event prior to the observed overestimation.

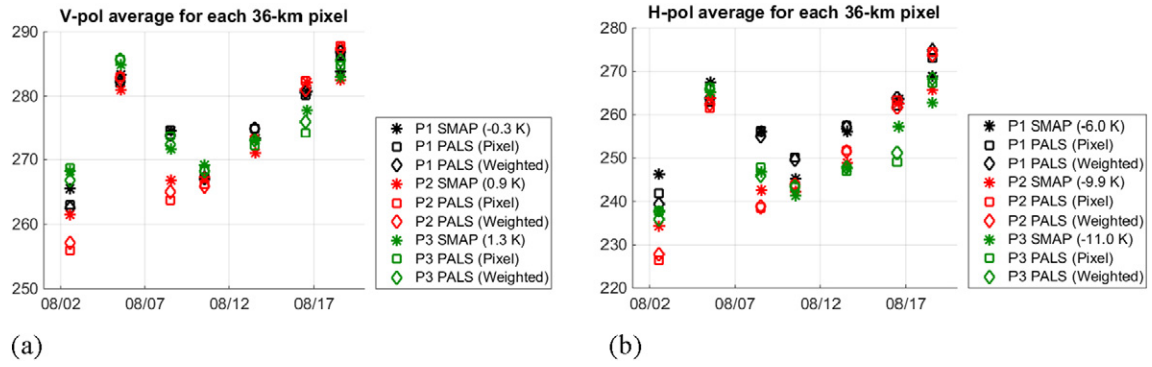

Fig. 4. Comparison of SMAP and PALS brightness temperatures over each of the 36-km pixels (P1 through P3) in the experiment domain for (a) vertical and (b) horizontal polarization. The mean difference between PALS (computed using the weighting scheme) and SMAP in each pixel is removed from the plots and showed in the legend in parenthesis next to "SMAP". "Pixel" refers to arithmetic average of PALS brightness temperature within the SMAP pixel and "Weighted" refers to Gaussian-weighted average.

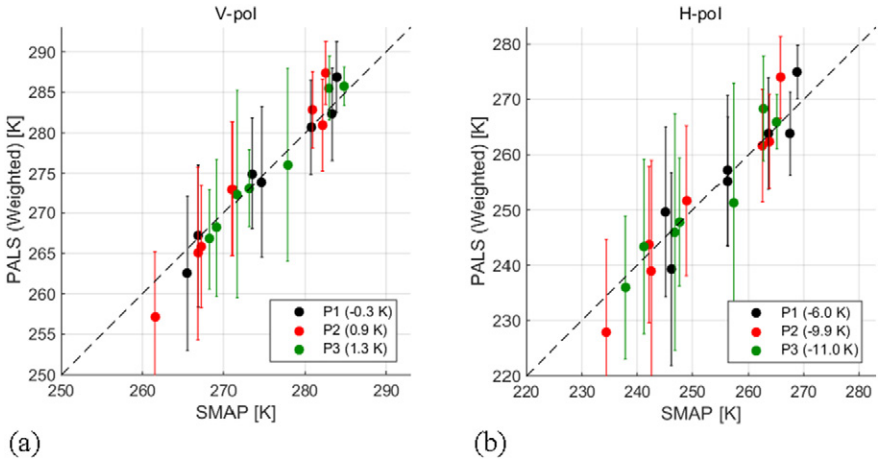

Fig. 5. Comparison of SMAP and PALS brightness temperatures over each of the 36-km pixels (P1 through P3) in the experiment domain for (a) vertical and (b) horizontal polarization. The PALS brightness temperature is computed using the Gaussian weighted average. The mean difference for each pixel is removed from the plots and displayed in the legend. The error bars show the standard deviation of the brightness temperature within the pixel as determined from the PALS 1-km measurements.

Pixels 1 and 4 had outliers on the third flight day. In pixel 1, station P04 responded to the precipitation event but the rest of the stations did not exhibit this increase in soil moisture; for example, the gauge at P03 detected <1 mm rain whereas P04 logged about 6 mm of rain (the precipitation of the individual stations is not shown in the plots). As mentioned above, the manual sample at P04 did not show an increase in the soil moisture. In pixel 4, neither the soil moisture sensor or rain gauge at P09 responded to the precipitation event detected by P06, which was almost 9 mm of rain, but the manual sample at P09 was clearly elevated. P09 is located at the edge of the pixel and even if

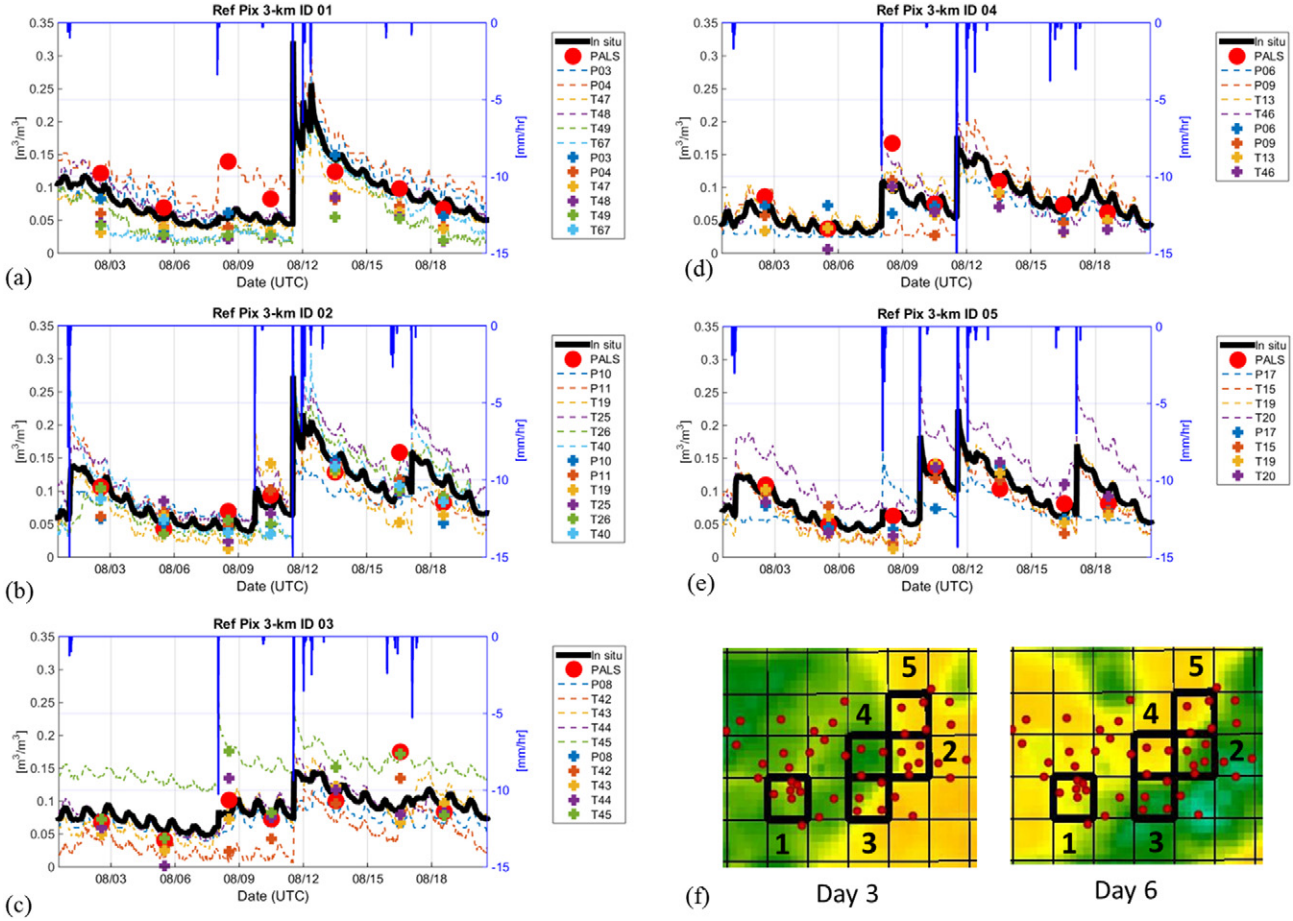

Fig. 6. (a)–(e) *In situ* measurement based soil moisture for the 3-km validation pixels and the PALS derived soil moisture over the pixels. The hourly precipitation is the average of the rain gauges within pixel collocated with the soil moisture sensors. The soil moisture reading of each station contributing to the validation pixel is plotted with dashed lines and the averages of manually sampled soil moisture at each station is shown with thick plus signs (P stands for permanent station; T stands for temporary station). (f) Map of the 3-km validation pixels where there are at least four soil moisture sensors within pixels with the PALS soil moisture from the third and the sixth flight days as the background. The red dots indicate the soil moisture sensors and thick black lines mark the validation pixels (thin black lines indicate the SMAP 3-km grid).

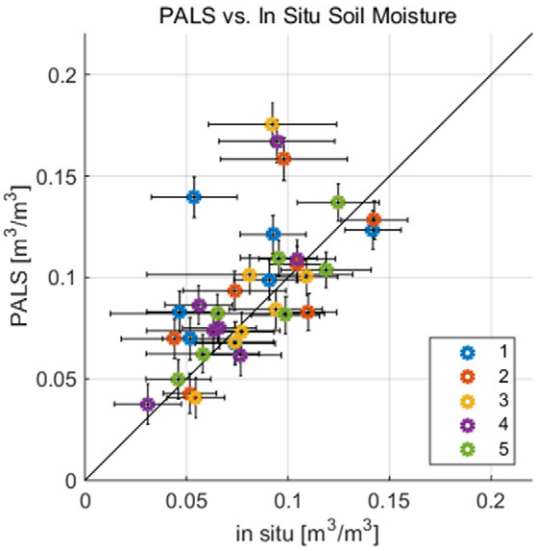

Fig. 7. *In situ* measurement based soil moisture for the 3-km validation pixels with respect to the PALS derived soil moisture over the pixels.

the edge was dry it may be that the majority of the pixel was wet – a situation which was also supported by the PALS soil moisture map. This would resulted in P09 misrepresenting almost 25% of the pixel, which would result in the overestimation observed. As of now, we have no explanation for the inconsistencies between the stations and the manual sampling, but overall (as discussed) there is a rationale as to why the PALS soil moisture deviates from the ground measurements in these cases.

In pixels 2 and 3, the outliers are found on the sixth flight day. In pixel 2, P10, P11, T25 and T26 logged between 2 mm and 5 mm of rain prior to the PALS flights. Only in the case of T26 did the soil moisture sensor show a notable response to the rain. T19 did not record any precipitation at that time and at T40 the rain gauge was not operating. For pixel 3, the overestimation occurred on the sixth flight day. The soil moisture measurement of station T42 was the only one that shows a clear increase corresponding to the PALS observed soil moisture. The manual sampling also captured this change. However, the precipitation measurements revealed that all the stations in the pixel except P08 had some precipitation prior to the PALS observation. This is a similar situation as found in the case of pixel 2. Both pixels were found on the edge of the soil moisture gradient which potentially contributed to the comparison in the same way as in the case of pixel 1 and 4 above. Furthermore, microwave observations are most sensitive to the moisture in the top layer of the soil while the *in situ* sensors are centered at a 5-cm depth. In this case, it is possible that the relatively small amount of water in the top surface layer is observed by PALS but does not have much impact on the *in situ* sensors, the only exception being stations T26 in pixel 2 and T42 in pixel 3. The lesser amount of rain recorded by the rain gauges at the other station is consistent with the fact that they seemed to be at the edge of the precipitation event.

There are additional reasons for discrepancies that include large rocks or soil voids that can direct any significant precipitation around a sensor. Another possible reason could be that when the sensor is inserted into the soil, it pinches the soil between the tines, essentially making it denser locally, which would divert any vertical infiltration around the sensor through the less dense soil surrounding the sensor. Finally, strong evaporation occurring at the surface after the rain may significantly diminish the amount of water reaching the sensors. Table 2 shows that the metrics are significantly improved if these four outliers are screened out.

The general conclusion is that the PALS soil moisture corresponds well to the events on the ground but it is not unexpected that there are discrepancies resulting from the mismatch in what each measures and heterogeneity of the soil moisture distribution. It is also noteworthy that the metrics before screening are close to those reported for the first 11 months of the mission by Colliander et al. (2017) for WGEW, which are also shown in Table 2. The validated soil moisture fields provided by PALS at 1.2-km resolution can be used to investigate the spatial scaling of the *in situ* measurements to SMAP resolution scale.

6.3. SMAP and PALS soil moisture vs. in situ

Fig. 8 shows the comparison of the SMAP radiometer-based soil moisture product (L2SMP), PALS soil moisture computed using *in situ* soil temperature and model-based soil temperature (see Section 4.2), and two different versions of the *in situ* soil moisture for the 36-km WGEW validation pixel. The two *in situ* soil moisture estimates are based on using two different sets of stations. One set includes only the permanent stations that have continuous measurements during the experiment (some of the stations used in computing the metrics by Chan et al. (2016) and Colliander et al. (2017) dropped out occasionally during the experiment period) and the other includes temporary stations deployed only during the field campaign. The Voronoi diagram (or Thiessen polygons, *e.g.*, Section 4.3 in Dingman, 2015) based weighted average was computed for both cases (see Fig. 9). Voronoi diagrams have been applied for validation of soil moisture products before (Jackson et al., 2010, 2012) and they were utilized also in the SMAP soil moisture product validation (Colliander et al., 2017). The PALS values were computed as an arithmetic average of the retrieved soil moisture within the pixel using the two methods. The precipitation amounts in Fig. 8 are based on the permanent stations; the differences between these and using all stations are not important in the context of the following discussion.

The average soil moisture based on all stations corresponded better to the precipitation events (increase in soil moisture after rain) when looking at the precipitation preceding the first and the sixth flight day (see the red vertical lines in Fig. 8). Fig. 10 shows that the SMAP and the two versions of the PALS soil moistures corresponded well to each other, which is also supported by the scatterplots shown in Fig. 11 and metrics listed in Table 3. This result was expected because, as shown previously, the brightness temperatures were close to each other (Section 6.1) and the soil moisture algorithms are similar (Sections 4.2 and 5). It is also evident that in this case the application of the model-based soil temperature resulted in very similar soil moisture values as when soil moisture was retrieved using the *in situ* measurement based soil temperature. However, the *in situ* sensors did not respond to the precipitation event just before the 3rd flight very well for either case (the yellow vertical line), but the SMAP and PALS observations, which include the near surface contribution, were impacted by the rain event because the retrieved soil moisture levels are elevated. This result is supported by the observations of the 3-km pixels in Fig. 6 where the *in situ* measurements showed a dampened response to the 3rd day precipitation event while the PALS retrievals experienced a clear increase in soil moisture. It is likely that differences between the rain gauge

Table 2
Metrics of the PALS soil moisture computed with respect to the 3-km pixels. RSMD stands for Root Square Mean Difference, ubRMSD stands for unbiased RMSD, and R stands for Pearson correlation.[a]

	All observations	Screened observations	11-month assessment[a]
ubRMSD [m^3/m^3]	0.028	0.016	0.028
Bias [m^3/m^3]	0.011	0.003	−0.006
RMSD [m^3/m^3]	0.030	0.016	0.028
R [−]	0.62	0.83	0.69

[a] Colliander et al. (2017)

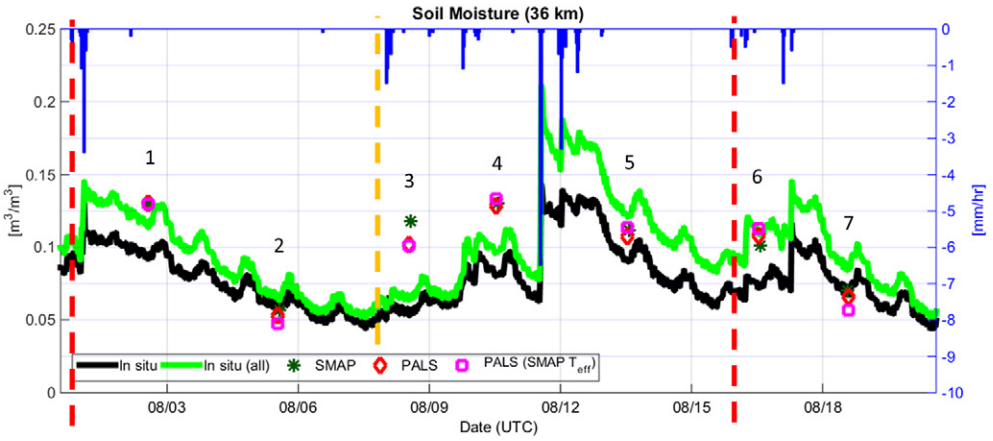

Fig. 8. Comparison of PALS and SMAP soil moistures at 36-km scale with respect to the *in situ* soil moisture. Black line is based on the average of the selected stations only; the green line is based on all stations, including temporary ones. The dashed red and yellow lines are used to highlight precipitation events that are discussed in the text.

estimates *versus* the *in situ* soil moisture estimates (see Section 6.2) contributed to this lack of correspondence.

On the fourth flight day (see Fig. 12), there was only one station in the bottom portion of the domain that was predominantly wetter than the top half (based on the PALS soil moisture), which corresponds to where the most stations are. The one station was weighted more according to the Voronoi diagrams but geographically did not account for the entire half (see Fig. 9). This may contribute to the PALS and SMAP soil moisture averages being higher than the *in situ* averages. At the same time, the average based on using all stations seemed to capture the wet spots in the top half better (based on the distribution of the stations and the location of the wet spots), which seemed to explain why using all stations has a higher average value during this time.

Overall the metrics were relatively good except for the correlation, which suffers from the small range of soil moisture (Table 3). The scatterplot shows the outliers on the third and fourth day for both SMAP and PALS soil moisture estimates. The PALS-derived high-resolution soil moisture provided the crucial information to explain these discrepancies between SMAP and *in situ* soil moisture, which yielded the conclusion that SMAP L2SMP provided valid soil moisture estimates during the experiment period.

7. Discussion

Spatial upscaling of *in situ* measurements is a critical aspect in validating remote sensing data products. In the case of the SMAP L2SMP data product the task is to estimate the average soil moisture over 36-km pixels with the point-wise *in situ* sensors. In the previous sections, the PALS measurements resolved the soil moisture distribution within the WGEW validation pixel at 1-km resolution during SMAPVEX15. The analysis showed that these measurements together with the augmented *in situ* observations exhibited some discrepancies between the SMAP L2SMP product and the average estimated by the permanent *in situ* sensors within the pixel. It was concluded that these discrepancies are due to the fact that the *in situ* sensors do not capture the vertical and horizontal dynamics of the soil moisture within the pixel in the same way as the radiometer measurements.

In terms of the vertical component, it is well-known that soil moisture determines the thickness of the soil layer that contributes to the observed brightness temperature (Njoku and Kong, 1977; Wilheit, 1978). The increased water content in the soil determines the permittivity which then increases for increasing water content. The assumption of the general correspondence between 5-cm *in situ* soil moisture

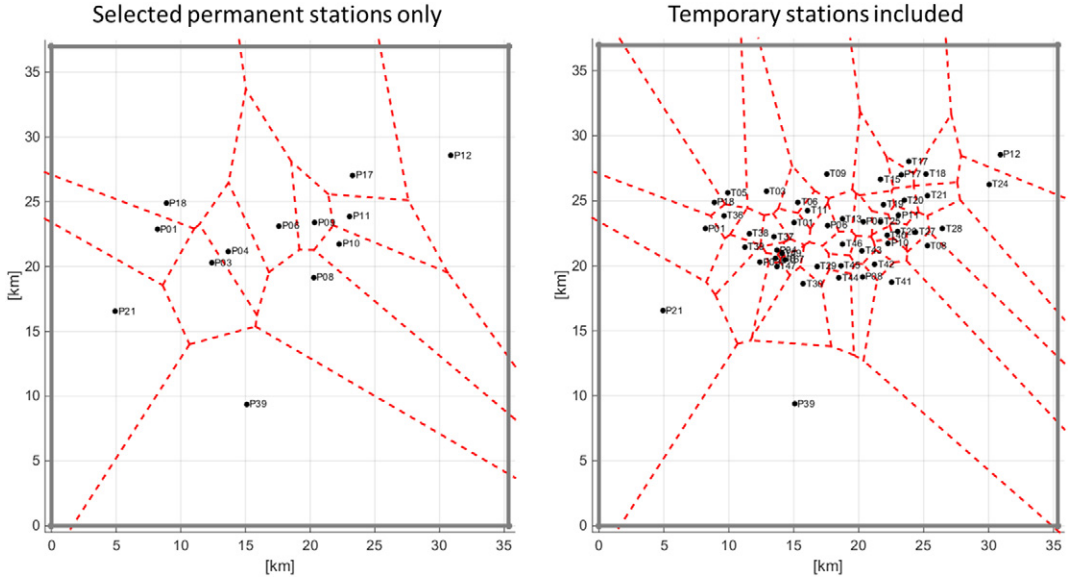

Fig. 9. Voronoi diagrams for the two sets of *in situ* sensors used for computing the average soil moisture for the 36-km pixel.

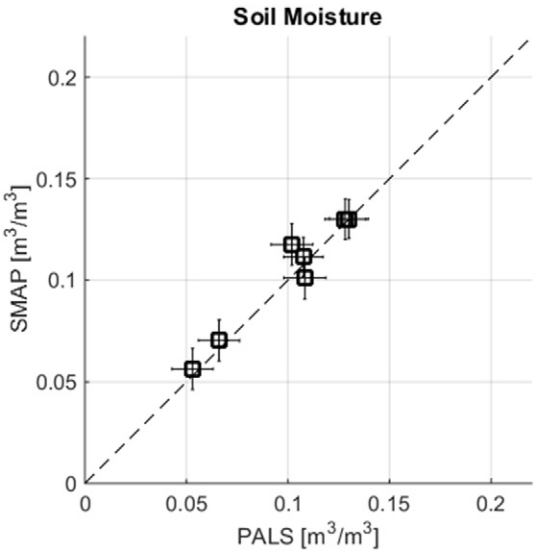

Fig. 10. PALS soil moisture *vs.* SMAP soil moisture over the WGEW 36-km pixel.

measurements and retrievals of soil moisture based on the microwave radiometer holds to the first order, in particular for L-band (*e.g.* Jackson et al., 2012; Kerr et al., 2016; Colliander et al., 2017). However, second-order differences in radiometer-based soil moisture retrieval and 5-cm *in situ* measurements have been reported in several previous studies. Escorihuela et al. (2010) used tower-based measurements to investigate soil moisture dynamics in the top surface and found that the effective sensing depth at L-band can be shallower than 5-cm. Rondinelli et al. (2015) used the SMOS data and an *in situ* network in Iowa (the South Fork core validation site) to show that the SMOS L-band radiometer based soil moisture estimates are sensitive to a shallower layer in the soil than the *in situ* sensors at 5-cm depth. Shellito et al. (2016) analyzed the dry-down rate of the SMAP L2SMP soil moisture over SMAP core validation sites and came to the conclusion that in general SMAP captures different dry-down dynamics than the *in situ* sensors installed at 5-cm depth. What these studies did not include was the evaluation on the correspondence of the soil moisture sensors with rain gauges as was done in this study, which verified the radiometer-based observations. The SMAP soil moisture products are defined as estimates of the soil moisture in the top 5-cm of the soil (Entekhabi et al., 2014). Therefore, even if the deviation of the data products from the *in situ* values can be explained by the difference in

Table 3
Soil moisture retrieval metrics for PALS and SMAP for two cases: permanent stations only and all stations including temporary stations.

	Permanent stations		All stations	
	PALS	SMAP	PALS	SMAP
ubRMSD [m^3/m^3]	0.022	0.023	0.021	0.025
Bias [m^3/m^3]	0.025	0.029	0.004	0.008
RMSD [m^3/m^3]	0.033	0.037	0.022	0.026
R [−]	0.59	0.49	0.64	0.49

the sensing depth the deviation is included in the product uncertainty under this definition. It is possible, however, to estimate the sensing depth separately before utilization of the soil moisture retrieval for an application where it may be critical (see, for example, Escorihuela et al., 2010). Accounting for the sensing depth in validation would effectively improve the data product performance by reducing systematic errors in the default metrics reported in Chan et al. (2016) and Colliander et al. (2017). Beyond the sensing depth it was discussed in Section 6.2 that the water may fail to infiltrate to the soil moisture probes under certain conditions. This is an uncertainty in the *in situ* measurement (as opposed to the remote sensing retrieval) and its impact on the computation of the remote sensing data product performance metrics should be minimized, as was done in Section 6.2 for the PALS soil moisture metrics. Furthermore, when the *in situ* measurements are applied to algorithm development, it is important to understand the mechanisms affecting the comparison between the *in situ* sensors and the retrieval algorithm so that the parameters of the algorithm are tuned for the correct reasons.

In terms of horizontal soil moisture dynamics, statistical models can be applied to compute how many points comprise an adequate *in situ* sampling. The results of Famiglietti et al. (2008) were used in SMAP soil moisture product validation planning (Colliander et al., 2017). However, the spatial variability of soil moisture is dependent on local conditions such as spatial distribution of soil type and vegetation cover, topographical variation, and precipitation patterns (Famiglietti et al., 1999). This study demonstrated the impact of heterogeneous sub-pixel precipitation on the estimation of the average soil moisture in a pixel where the number of *in situ* stations met the threshold of 8 stations set by SMAP (Section 6.3). The threshold was computed to obtain 70% confidence for 0.03 m^3/m^3 soil moisture uncertainty with 0.07 m^3/m^3 sub-pixel variability (Colliander et al., 2017). Based on the PALS 1-km data the variability within the WGEW pixel ranged from 0.024 m^3/m^3 to 0.066 m^3/m^3 during the experiment. While the statistical variability is within the specified range it is easy to see based on this

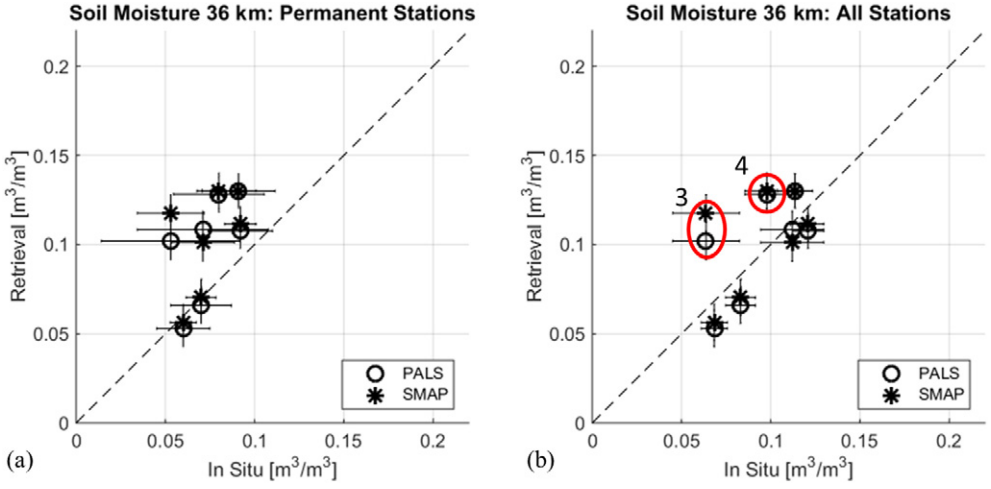

Fig. 11. Scatterplots of PALS and SMAP soil moistures at 36-km scale with respect to the average *in situ* soil moisture based on (a) the permanent stations only, and (b) all stations including temporary stations, with comparisons of the third and fourth flight day highlighted.

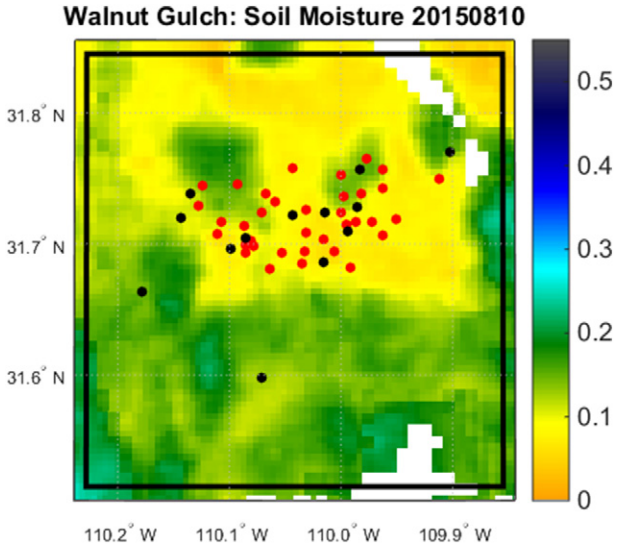

Fig. 12. PALS derived soil moisture with permanent stations (black) and temporary stations (red) on the fourth flight day.

study that it is possible to have individual cases where the number of stations is not adequate to capture the average soil moisture (and this is why the confidence interval is specified), especially in a region dominated by small convective rainfall cells. It is noted that the locations of the permanent stations at WGEW were determined based on hydrologic research objectives of the watershed and not optimized for the validation of the SMAP soil moisture data products. The distribution of the temporary network stations in 2015 was designed to augment the permanent network for capturing the fine spatial scale precipitation events and validating the high-resolution soil moisture products of SMAP, an objective which became obsolete upon the failure of the radar. Nevertheless, this is the reason why the temporary stations were not spread around the pixel more and there is only one station in the southern part in this case. An informed distribution of stations accounting for the desired validation resolution would mitigate an issue of this kind, but in order to improve the accuracy in the extreme cases of heterogeneity the straightforward approach would be to add more stations. However, this is not always practical. Other approaches, such as utilization of hydrological models (Crow et al., 2005; Coopersmith et al., 2015), can be applied to improve the accuracy of the soil moisture estimate provided by the network without deployment of additional resources in the field.

8. Conclusions

SMAPVEX15 was conducted in southeast Arizona in order to support the SMAP soil moisture data product calibration and validation activities. The experiment domain included the Walnut Gulch Experimental Watershed, which is a SMAP core validation site. The experiment included the collection of airborne radiometer and radar measurements and intensive ground sampling. This study focused on the radiometer measurements. The *in situ* measurements were used to validate the PALS radiometer-based soil moisture at 1-km resolution. The unbiased RMSD (root mean square difference) was estimated to be 0.030 m^3/m^3 and the Pearson correlation was 0.62. The comparisons also showed that the *in situ* soil moisture measurements did not always capture all the precipitation events correctly based on information from a dense network of rain gauges in the area. Removing those cases (approximately 10% of the observations) yielded significantly improved error statistics (RMSD 0.016 m^3/m^3 and correlation 0.83) for the PALS soil moisture. The challenge for routine validation is how to identify these conditions with the available data sources in near real time. PALS and SMAP soil moistures were found to be essentially similar owing to having similar brightness temperature measurements and soil moisture retrieval algorithms. However, there were discrepancies with respect to the *in situ* measurements. These discrepancies were associated with the soil moisture sensor deviations from rain gauges and with spatial heterogeneity, which was identified using the high-resolution PALS soil moisture and the intensive ground sampling. A source of error is the mismatch between the assumed sensing depth of the L-band radiometer-based soil moisture and the *in situ* probes at 5-cm depth. The SMAP soil moisture product definition acknowledges this by stating that 5-cm measurement depth of SMAP soil moisture retrievals is an approximate assumption. However, when *in situ* soil moisture sensors fail to represent the soil moisture at 5-cm depth it needs to be accounted for in the computation of the performance metrics as was done with the PALS soil moisture. The spatial heterogeneity of soil moisture was driven by precipitation patterns in SMAPVEX15, which caused significant uncertainties in the comparisons between *in situ* sensors and soil moisture retrieval at 36-km scale. The confidence in these comparisons can be improved by increasing the number of stations or augmenting the *in situ* based soil moisture average with a hydrological model. These conclusions indicate that the metrics computed for the SMAP radiometer-based soil moisture product over WGEW suffered from uncertainties greater than expected. This is of greatest importance during the monsoon season when the spatial distribution of soil moisture is especially heterogeneous. However, even with these uncertainties, the retrieval accuracy is still quite good.

Acknowledgments

The research described in this publication was carried out at the Jet Propulsion Laboratory, California Institute of Technology, under a contract with the National Aeronautics and Space Administration. Data sets from SMAPVEX15 will be made available through the National Snow and Ice Data Center (NSIDC). Landsat 8 data is available from the U.S. Geological Survey. The U.S. Department of Agriculture is an equal opportunity provider and employer. Finally, we would like to thank all the participants of SMAPVEX15 who made the experiment a success.

References

Adams, D.K., Comrie, A.C., 1997. The North American monsoon. Bull. Am. Meteorol. Soc. 78 (10), 2197–2213.
Barber, M., Bruscantini, C., Grings, F., Karszenbaum, H., 2016. Bayesian combined active/passive (B-CAP) soil moisture retrieval algorithm. J. Sel. Topics Appl. Rem. Sens. 9 (12), 5449–5460.
Bindlish, R., Jackson, T.J., Gasiewski, A., Stankov, B., Klein, M., Cosh, M.H., Mladenova, I., Watts, C., Vivoni, E., Lakshmi, V., Bolten, J., Keefer, T., 2008. Aircraft based soil moisture retrievals under mixed vegetation and topographic conditions. Remote Sens. Environ. 112 (2), 375–390.
Bindlish, R., Jackson, T., Sun, R., Cosh, M., Yueh, S., Dinardo, S., 2009. Combined passive and active microwave observations of soil moisture during CLASIC. IEEE Geosci. Rem. Sens. Lett. 6 (4), 644–648.
Bircher, S., Balling, J.E., Skou, N., Kerr, Y.H., 2012. Validation of SMOS brightness temperatures during the HOBE airborne campaign, Western Denmark. IEEE Trans. Geosci. Rem. Sens. 50 (5), 1468–1482.
Brodzik, M.J., Billingsley, B., Haran, T., Raup, B., Savoie, M.H., 2012. EASE-grid 2.0: incremental but significant improvements for earth-gridded data sets. ISPRS Int. J. Geogr. Inf. Sci. 1 (1), 32–45.
Burgin, M.S., Colliander, A., Njoku, E.G., Chan, S.K., Cabot, F., Kerr, Y., Bindlish, R., Jackson, T., 2017. A comparative study of the SMAP passive soil moisture product with existing satellite-based soil moisture products. IEEE Trans. Geosci. Remote Sens. (2017, Early Access).
Chan, S., Bindlish, R., Hunt, R., Jackson, T., Kimball, J., 2013. Soil moisture active passive (SMAP) - ancillary data report: vegetation water content. Jet Propulsion Laboratory. California Institute of Technology (JPL D-53016, January 21, 2013).
Chan, S., Njoku, E.G., Colliander, A., 2014. SMAP algorithm theoretical basis document (ATBD) level-1C radiometer data product (L1C_TB). SMAP Project. Jet Propulsion Laboratory, Pasadena, CA.
Chan, S., Bindlish, R., O'Neill, P., Njoku, E., Jackson, T.J., Colliander, A., Chen, F., Burgin, M., Dunbar, R.S., Piepmeier, J., Yueh, S., Entekhabi, D., Cosh, M.H., Seyfried, M.S., Bosch, D.D., Starks, P., Goodrich, D.C., Prueger, J.H., Crow, W.T., Caldwell, T., Walker, J., Wu, X., Pacheco, A., McNairn, H., Anderson, M.C., 2016. Assessment of the SMAP Level 2 passive soil moisture product. IEEE Trans. Geosci. Rem. Sens. 54 (8), 4994–5007.

Chen, F., Crow, W.T., Colliander, A., Cosh, M.H., Jackson, T.J., Bindlish, R., Reichle, R.H., Chan, S.K., Bosch, D.D., Starks, P.J., Goodrich, D.C., Seyfried, M.S., 2017. Application of triple collocation in ground-based validation of soil moisture active/passive (SMAP) level 2 data products. IEEE J. Sel. Topics Appl. Earth Obs. Remote Sens. 10 (2), 489–502.

Choudhury, B.J., Schmugge, T.J., Chang, A., Newton, R.W., 1979. Effects of surface roughness on the microwave emission from Soils. J. Geophys. Res. 84 (C9), 5699–5706.

Colliander, A., Chan, S., Kim, S.-B., Das, N., Yueh, S., Cosh, M., Bindlish, R., Jackson, T., Njoku, E., 2012. Long term analysis of PALS soil moisture campaign measurements for global soil moisture algorithm development. Rem. Sens. Env. 121, 309–322.

Colliander, A., Jackson, T.J., McNairn, H., Chazanoff, S., Dinardo, S., Latham, B., O'Dwyer, I., Chun, W., Yueh, S., Njoku, E., 2015. Comparison of airborne passive and active L-band System (PALS) brightness temperature measurements to SMOS observations during the SMAP validation experiment 2012 (SMAPVEX12). IEEE Geosci. Rem. Sens. Lett. 12 (4), 801–805.

Colliander, A., Njoku, E.G., Jackson, T.J., Chazanoff, S., McNairn, H., Powers, J., Cosh, M.H., M.H., 2016a. Retrieving soil moisture for non-forested areas using PALS radiometer measurements in SMAPVEX12 field campaign. Rem. Sens. Env. 184, 86–100.

Colliander, A., Jackson, T.J., Bindlish, R., Chan, S., et al., 2017. Validation of SMAP surface soil moisture products with core validation sites. Rem. Sens. Env. 191, 215–231.

Coopersmith, E.J., Cosh, M.H., Petersen, W.A., Prueger, J., Niemeier, J., 2015. Soil moisture model calibration and validation: an ARS watershed on the South Fork Iowa River. J. Hydrometeorol. 16, 1087–1101.

Cosh, M.H., Jackson, T.J., Bindlish, B., Famiglietti, J.S., Ryu, D., 2005. Calibration of an impedance probe for estimation of surface soil water content over large regions. J. Hydrol. 311 (1–4), 49–58.

Cosh, M.H., Jackson, T.J., Moran, S., Bindlish, R., 2008. Temporal persistence and stability of surface soil moisture in a semi-arid watershed. Remote Sens. Environ. 112, 304–313.

Crow, W.T., Ryu, D., Famiglietti, J.S., 2005. Upscaling of field scale soil moisture measurements using distributed land surface modeling. Adv. Water Resour. 28, 1–14.

Dingman, S.L., 2015. Physical fHydrology. Waveland Press, Inc., Illinois, USA.

Entekhabi, D., Yueh, S., O'Neill, P., Kellogg, K., 2014. SMAP handbook – soil moisture active passive: mapping soil moisture and freeze/thaw from space. SMAP Project. Jet Propulsion Laboratory, Pasadena, CA.

Escorihuela, M.J., Chanzy, A., Wigneron, J.P., Kerr, Y.H., 2010. Effective soil moisture sampling depth of L-band radiometry: a case study. Remote Sens. Environ. 114, 995–1001.

Famiglietti, J.S., Devereaux, J.A., Laymon, C.A., Tsegaye, T., Houser, P.R., Jackson, T.J., Graham, S.T., Rodell, M., van Oevelen, P.J., 1999. Ground-based investigation of soil moisture variability within remote sensing footprints during the Southern Great Plains 1997 (SGP97) Hydrology Experiment. Water Resour. Res. 35 (6), 1839–1851.

Famiglietti, J.S., Ryu, D., Berg, A.A., Rodell, M., Jackson, T.J., 2008. Field observations of soil moisture variability across scales. Water Resour. Res. 44, W01423.

Goodrich, D.C., Keefer, T.O., Unkrich, C.L., Nichols, M.H., Osborn, H.B., Stone, J.J., Smith, J.R., 2008. Long-term precipitation database, Walnut Gulch Experimental Watershed, Arizona, United States. Water Resour. Res. 44, W05S04.

Jackson, T.J., 1993. Measuring surface soil moisture using passive microwave remote sensing. Hydrol. Process. 7, 139–152.

Jackson, T.J., Schmugge, T.J., 1991. Vegetation effects on the microwave emission of soils. Rem. Sens. Env. 36, 203–212.

Jackson, T.J., Cosh, M.H., Bindlish, R., Starks, P.J., Bosch, D.D., Seyfried, M., Goodrich, D.C., Moran, M.S., Du, J., 2010. Validation of advanced microwave scanning radiometer soil moisture products. IEEE Trans. Geosci. Rem. Sens. 48 (12).

Jackson, T.J., Bindlish, R., Cosh, M.H., Zhao, T., Starks, P.J., Bosch, D.D., Seyfried, M., Moran, M.S., Goodrich, D.C., Kerr, Y.H., Leroux, D., 2012. Validation of Soil Moisture and Ocean Salinity (SOMS) Soil Moisture Over Watershed Networks in the U.S. IEEE Trans. Geosci. Rem. Sens. 50 (5).

Jackson, T.J., Colliander, A., Kimball, J., Reichle, R., Crow, W., Entekhabi, D., O'Neill, P., Njoku, E., 2013. SMAP science data calibration and validation plan. SMAP Mission. D-52544 JPL (April 2, 2013).

Keefer, T.O., Moran, M.S., Paige, G.B., 2008. Long-term meteorological and soil Hydrology database, Walnut Gulch Experimental Watershed, Arizona, United States. Water Resour. Res. 44.

Kerr, Y.H., Al-Yaari, A., Rodriguez-Fernandez, N., Parrens, M., et al., 2016. Overview of SMOS performance in terms of global soil moisture monitoring after six years in operation. Remote Sens. Environ. 40–63.

Kustas, W.P., Moran, M.S., Humes, K.S., Stannard, D.I., Pinter Jr., P.J., Hipps, L.E., Swiatek, E., Goodrich, D.C., 1994. Surface energy balance estimates at local and regional scales using optical remote sensing from an aircraft platform and atmospheric data collected over semiarid rangelands. Water Resour. Res. 30 (5), 1241–1259.

Kirdiashev, K.P., Chukhlantsev, A.A., Shutko, A.M., 1979. Microwave radiation of the Earth's surface in the presence of vegetation. Radio Eng. Electron. USSR 24, 256–264.

Le Vine, D., Lagerloef, G., Colomb, F., Yueh, S., Pellerano, F., 2007. Aquarius: An instrument to Monitor Sea surface salinity from space. IEEE Trans. Geosci. Rem. Sens. 45 (7), 2040–2050.

Magagi, R., et al., 2013. Canadian experiment for soil moisture in 2010 (CanEx-SM10): overview and preliminary results. IEEE Trans. Geosci. Rem. Sens. 51 (1).

McNairn, H., Jackson, T., Wiseman, G., Belair, S., Berg, A., Bullock, P., Colliander, A., Cosh, M., Kim, S., Magagi, R., et al., 2015. The soil moisture active passive validation experiment 2012 (SMAPVEX12): pre-launch calibration and validation of the SMAP satellite. IEEE Trans. Geosci. Rem. Sens. 53 (5).

Mironov, V.L., Kosolapova, L.G., Fomin, S.V., 2009. Physically and Mineralogically based spectroscopic dielectric model for moisture Soils. IEEE Trans. Geosci. Rem. Sens. 47 (7), 2059–2070.

Misra, S., et al., 2017. Radiometric calibration of the airborne rotating passive and active L-band system (PALS). IEEE Geosci. Remote Sens. Lett. (Submission).

Moran, M.S., Emmerich, W.E., Goodrich, D.C., Heilman, P., Holifield Collins, C., Keefer, T.O., Nearing, M.A., Nichols, M.H., Renard, K.G., Scott, R.L., Smith, J.R., Stone, J.J., Unkrich, C.L., Wong, J.K., 2008. Preface to special section on Fifty years of research and data collection: U.S. Department of Agriculture Walnut Gulch Experimental Watershed. Water Resour. Res. 44, W05S01. http://dx.doi.org/10.1029/2007WR006083.

Narayan, U., Lakshmi, V., Njoku, E., 2004. Retrieval of soil moisture from passive and active L/S band sensor (PALS) observations during the soil moisture experiment in 2002 (SMEX02). Rem. Sens. Env. 92, 483–496.

Njoku, E.G., Kong, J.-A., 1977. Theory for passive microwave remote sensing of near-surface soil moisture. J. Geophys. Res. 82 (20), 3108–3118.

Njoku, E.G., Entekhabi, D., 1996. Passive microwave remote sensing of soil moisture. J. Hydrol. 184, 101–129.

Njoku, E.G., Wilson, W.J., Yueh, S.H., Dinardo, S.J., Li, F.K., Jackson, T.J., Lakshmi, V., Bolten, J., 2002. Observations of soil moisture using a passive and active low frequency microwave airborne sensor during SGP99. IEEE Trans. Geosci. Rem. Sens. 40 (12), 2659–2673.

O'Neill, P., Chan, S., Njoku, E.G., Jackson, T.J., Bindlish, R., 2016. Algorithm Theoretical Basis Document Level 2 & 3 Soil Moisture (Passive) Data Products, Rev. C. SMAP Project, JPL D-66480, December 15, 2016. Jet Propulsion Laboratory, Pasadena, CA.

Pan, M., Cai, X., Chaney, N.W., Entekhabi, D., E. F., 2016. Wood. An initial assessment of SMAP soil moisture retrievals using high-resolution model simulations and in situ observations. Geophys. Res. Lett. 43, 9662–9668.

Panciera, R., Walker, J.P., Jackson, T.J., Gray, D.A., Tanase, M.A., Ruy, D., Monerris, A., Yardley, H., Rudiger, C., Wu, X., et al., 2014. The soil moisture active passive experiments (SMAPEx): Toward soil moisture retrieval from the SMAP mission. IEEE Trans. Geosci. Rem. Sens. 52, 490–507.

Piepmeier, J.R., Focardi, P., Horgan, K.A., Knuble, J., Ehsan, N., Lucey, J., Brambora, C., Brown, P.R., et al., 2017. SMAP L-band microwave radiometer: Instrument design and first year on orbit. IEEE Trans. Geosci. Rem. Sens. 55 (4), 1954–1966.

Piepmeier, J., Mohammed, P., De Amici, G., Kim, E., Peng, J., Ruf, C., 2016. SMAP Algorithm Theoretical Basis Document (ATBD) L1B Radiometer Brightness Temperature Data Product: L1B_TB. SMAP Project, Goddard Space Flight Center, Greenbelt, MD.

Rondinelli, W.J., Hornbuckle, B.K., Patton, J.C., Walker, V.A., Carr, B.D., Logsdon, S.D., 2015. Different rates of soil drying after rainfall are observed by the SMOS satellite and the South Fork in situ soil moisture network. J. Hydrometeorol. 16, 889–903.

Rowlandson, T.L., Berg, A.A., Bullock, P.R., Ojo, E.R., McNairn, H., Wiseman, G., Cosh, M.H., 2013. Evaluation of several calibration procedures for a portable soil moisture sensor. J. Hydrol. 498, 335–344.

Shellito, P.J., Small, E.E., Colliander, A., Bindlish, R., Cosh, M.H., Berg, A., Bosch, D.D., Caldwell, T.G., Goodrich, D.C., McNairn, H., Prueger, J., Starks, P.J., van der Velde, R., Walker, J., 2016. SMAP soil moisture drying more rapid than observed in situ following rainfall events. Geophys. Res. Lett. (Under Review).

Smith, S.W., 1997. The Scientist and Engineer's Guide to Digital Signal Processing. 1997. California Technical Publishing, San Diego, California, USA.

Srivastava, P.K., O'Neill, P., Cosh, M., Kurum, M., Lang, R., Joseph, A., 2015. Evaluation of dielectric mixing models for passive microwave soil moisture retrieval using data from ComRAD ground-based SMAP simulator. IEEE J. Sel. Top. App. Earth. Obs. Remote Sens. 8 (9), 4345–4354.

Tanner, A., Wilson, W., Pellerano, F., 2003. Development of a high stability L-band radiometer for ocean salinity measurements. Proc. IEEE Geosci. Rem. Symp. 1238–1240.

Ye, N., Walker, J., Wu, X., Jackson, T., Renzullo, L., Merlin, O., Rudiger, C., Entekhabi, D., DeJeu, R., Kim, E., 2016. Towards Validation of SMAP: SMAPEx-4 & -5. Proc. IEEE Int. Geosci. Rem. Sens. Symp., Beijing, China, July 10–15, 2016.

Yueh, S., Dinardo, S., Chan, S., Njoku, E., Jackson, T., Bindlish, R., 2008. Passive and Active L-Band System and Observations during the 2007 CLASIC Campaign. Proc. IEEE Int. Geosci. Rem. Sens. Symposium 2008. 2, pp. 7–11 (pp. II-241 - II-244).

Wilheit, T., 1978. Radiative transfer in a plane stratified dielectric. IEEE Trans. Geosci. Electron. GE-16, 138–143.

Wilson, W., Yueh, S., Dinardo, S., Chazanoff, S., Kitiyakara, A., Li, F., Rahmat-Samii, Y., 2001. Passive active L- and S-band (PALS) microwave sensor for ocean salinity and soil moisture measurements. IEEE Trans. Geosci. Rem. Sens. 39 (5), 1039–1048.